Received: 28 July 2021 | Revised: 8 December 2021 | Accepted: 29 December 2021

DOI: 10.1002/mp.15449

RESEARCH ARTICLE

MEDICAL PHYSICS

Beam properties within the momentum acceptance of a clinical gantry beamline for proton therapy

Anna Chiara Giovannelli[1,2] | **Vivek Maradia**[1,2] | **David Meer**[1] | **Sairos Safai**[1] | **Serena Psoroulas**[1] | **Michele Togno**[1] | **Christian Bula**[1] | **Damien Charles Weber**[1,3,4] | **Antony John Lomax**[1,2] | **Giovanni Fattori**[1]

[1] Center for Proton Therapy, Paul Scherrer Institut, Villigen, Switzerland

[2] Department of Physics, ETH Zürich, Zürich, Switzerland

[3] University Hospital Zürich, Zürich, Switzerland

[4] University Hospital Bern, University of Bern, Bern, Switzerland

Correspondence
Anna Chiara Giovannelli, Center for Proton Therapy, Paul Scherrer Institut, Forschungsstrasse 111, WBBB/105, 5232 Villigen PSI, Switzerland.
Email: anna-chiara.giovannelli@psi.ch

Funding information
Swiss National Science Foundation, Grant/Award Number: 185082

Abstract

Purpose: Energy changes in pencil beam scanning proton therapy can be a limiting factor in delivery time, hence, limiting patient throughput and the effectiveness of motion mitigation techniques requiring fast irradiation. In this study, we investigate the feasibility of performing fast and continuous energy modulation within the momentum acceptance of a clinical beamline for proton therapy.

Methods: The alternative use of a local beam degrader at the gantry coupling point has been compared with a more common upstream regulation. Focusing on clinically relevant parameters, a complete beam properties characterization has been carried out. In particular, the acquired empirical data allowed to model and parametrize the errors in range and beam current to deliver clinical treatment plans.

Results: For both options, the local and upstream degrader, depth-dose curves measured in water for off-momentum beams were only marginally distorted (γ(1%, 1 mm) > 90%) and the errors in the spot position were within the clinical tolerance, even though increasing at the boundaries of the investigated scan range. The impact on the beam size was limited for the upstream degrader, while dedicated strategies could be required to tackle the beam broadening through the local degrader. Range correction models were investigated for the upstream regulation. The impaired beam transport required a dedicated strategy for fine range control and compensation of beam intensity losses. Our current parameterization based on empirical data allowed energy modulation within acceptance with range errors (median 0.05 mm) and transmission (median –14%) compatible with clinical operation and remarkably low average 27 ms dead time for small energy changes. The technique, tested for the delivery of a skull glioma treatment, resulted in high gamma pass rates at 1%, 1 mm compared to conventional deliveries in experimental measurements with about 45% reduction of the energy switching time when regulation could be performed within acceptance.

Conclusions: Fast energy modulation within beamline acceptance has potential for clinical applications and, when realized with an upstream degrader, does not require modification in the beamline hardware, therefore, being potentially applicable in any running facility. Centers with slow energy switching time can particularly profit from such a technique for reducing dead time during treatment delivery.

KEYWORDS
gantry, momentum acceptance, pencil beam scanning, proton therapy, treatment delivery

1 | INTRODUCTION

Brought into clinical practice at Paul Scherrer Institut (PSI) in the 1990s,[1] and further refined a few years later at GSI Helmholtzzentrum für Schwerionenforschung,[2] pencil beam scanning (PBS) is nowadays the standard beam delivery technique in charged particle radiotherapy. Even the most complicated geometries can be treated precisely with PBS, scanning a thin pencil beam across the target to deposit individually optimized dose spots and build dose in the patient. In this process, the clinical target is covered as a sequence of spot layers delivered at different depths, progressively changing the beam energy. The beam momentum variation between consecutive energy layers is typically around 1%.[3] Depending on the specific machine in use, such energy changes may take more than 1 s and are one of the main sources of dead time during the treatment delivery. In gantry-based proton facilities using cyclotrons, the bottleneck is typically more in the regulation of the large bending dipoles required to transport the beam to isocenter, than on the accelerator and energy degradation side. Achromatic gantry designs, however, allow particles with non-nominal momentum within a defined acceptance to be transported without chromatic dispersion, while keeping focus at isocenter. Despite such beamlines having finite momentum acceptance in the order of few percent dp/p, this is typically not exploited for energy regulation. Instead, the beam energy spectra is precisely defined to ensure fine control of range and beam position at isocenter. New medical beamline designs, featuring superconductive magnets, are, however, under investigation, obviating the need for regulating dipole settings, while, nevertheless, allowing for energy regulation within large momentum acceptances.[4]

Making the energy changes fast has a tangible impact in proton therapy for several reasons. First, it allows for shorter treatment times, which in turn is beneficial for patient comfort, treatment uncertainties, and running costs.[5] Moreover, PBS is particularly vulnerable to intrafractional organ motion, which can cause dose blurring and distortions due to the dynamic interplay effect with the scanning beam. If less time is needed to scan through the target volume, motion mitigation techniques like gating,[6] breath-hold,[7] and rescanning,[8–10] in particular, can be implemented more efficiently. Finally, having fast energy changes facilitates online adaptation of the beam settings such as to follow the patient anatomical variation in real-time, reigniting the potential of a clinical translation of tumor tracking techniques[3] for motion mitigation.

In particle therapy centers, cyclotrons, with fixed extraction energy, or synchrotrons, which can adjust energy pulse-to-pulse, are used. The typical time requirements for changing the energy in clinical facilities are reviewed in Table 1 and lie between seconds and hundreds of milliseconds. Usually a weak point of synchrotron-based facilities, a considerable amount of work has been done recently to develop multiple energy extraction, an approach studied at the Heavy Ion Medical Accelerator in Chiba (HIMAC)[11] and at Mayo Clinic Rochester and Arizona, bringing the switching time from 2 s close to 200 ms. A different strategy was investigated at GSI Helmholtzzentrum für Schwerionenforschung, where the energy switching time has been reduced down to 16 ms using a downstream degradation system.[12] In cyclotron-based beamlines, the extracted energy is fixed and lower energies are obtained slowing down particles by means of an absorber of variable thickness, a so-called energy degrader. The degrader can be located upstream,[13] just after the extraction of the beam from the accelerator, or downstream, before the patient in the treatment nozzle.[1] When an upstream degrader is used, all downstream magnets and energy selection systems, when available, need to follow these energy changes. In synchrotron-based facilities, the beam energy is set directly at the

TABLE 1 Overview of typical energy change times in clinical facilities

Institution	Accelerator	Energy change time	Reference
MD Anderson	Synchrotron	2000 ms	Smith et al.[16]
Mayo Clinic	Synchrotron	2000 ms	Shen et al.[17]
Mayo Clinic (Multiple energy extraction)		220 ms	Younkin et al.[18]
GSI	Synchrotron	1500 ms	Bert and Rietzel[15]
GSI (Downstream degrader)		16 ms	Saito et al.[12]
CNAO	Synchrotron	1000 ms	Biscari and Falbo[19]
HIMAC (Multiple energy extraction)	Synchrotron	200 ms	Mizushima et al.[11]
IBA Proteus®ONE	Cyclotron	900 ms	Pidikiti et al.[20]
Varian ProBeam 360°	Cyclotron	200–800 ms	Farr et al.[21]
PSI – G2	Cyclotron	80–100 ms	Pedroni et al.[13]

accelerator instead, but the switching time is typically longer than cyclotron-based setups. Therefore, for particularly demanding applications, the use of a downstream degrader has been investigated, with results matching the timing requirements for depth scanning[14] and 4D treatments.[15] In addition, exploiting the momentum acceptance of typical gantry systems, albeit limited in comparison to the aforementioned studies on superconductivity, is an option to achieve ultra-fast and continuous energy regulation, at least for moderate changes of beam range. Moreover, this approach does not necessarily require a degrader downstream of the nozzle and, therefore, is potentially applicable in most clinical units in operation. On the other hand, there will be inevitable effects on beam characteristics if they are varied within this acceptance, the magnitude of which needs to be understood before such an approach could be exploited.

In this study, therefore, we present the characterization of the beam properties within the momentum acceptance of the medical beamline and second-generation clinical gantry (Gantry 2) in operation at PSI since 2013.[22] With this experimental study, we wish to answer the following questions:

- At the current state of technology, can the beamline acceptance be exploited for fast and continuous energy regulation?
- What is the impact of such an approach on clinically relevant parameters like beam width, spot position accuracy, depth-dose profiles, and transmission?

2 | MATERIALS AND METHODS

2.1 | The Gantry 2 facility at PSI

The technical realization and commissioning of Gantry 2 can be found in several publications[1,23] and patents.[24,25] In the following, we briefly describe the components involved in beam energy selection and position control, which are relevant to this study.

A simplified schematic of the PROSCAN proton therapy facility at PSI is shown in Figure 1. A dedicated superconducting cyclotron from Varian[26] accelerates protons to 250 MeV. The extracted beam current is then regulated at the accelerator using a vertical electrostatic deflector installed near the ion source, which allows low latency beam current control at a time scale of 0.1 ms.[27] Energy changes are set by an upstream degrader consisting of two opposed sets of carbon wedges, whose relative position determines the amount of degrading material in the beamline.[28]

Following the degrader, the energy selection system uses a double bend symmetric achromatic system, with a horizontal focus at the symmetry point. Mechanical slits are used to cut the momentum acceptance and thus select the energy spectra of the beam transported

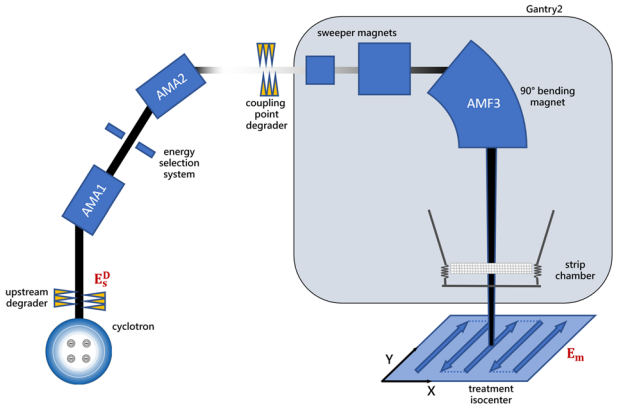

FIGURE 1 Schematic view of key elements for energy regulation and beam steering of the Gantry 2 beamline at Paul Scherrer Institut (CH). We will refer to E_m as the residual energy measured at the exit of the nozzle and to E_s^D as the energy (E) setpoint (s) of the upstream degrader (D)

further in the beamline.[29,30] The gantry beamline layout consists of three dipoles and two sweeper magnets located, respectively, at 4.6 and 5.2 m distance from isocenter for the X and Y scanning directions. The entire layout is optimized to obtain parallel beam with upstream scanning across ±10 cm (X direction) and ±6 cm (Y direction) field size.[13] The energy selection system and final bending section are designed to provide corrections to chromatic aberrations, making the whole beamline globally achromatic. In particular, the energy selection system is designed to allow a momentum acceptance dp/p of ±0.6%, within which particles are transported without chromatic dispersion, while being focused at isocenter.

The rotating beamline on the gantry is separated from the upstream fixed branch by an air gap of ca. 40 cm. Of those, 27 mm could be used as shown in Figure 1 to place a local degrader at the coupling point, the potential of which will be investigated in this work.

Based on commissioning data, changing beam energy in Gantry 2 under clinical settings takes around 100–80 ms,[23] ultimately limited by the two dipoles in the energy selection system (designated AMA1 and AMA2 at our facility), and the last 90° dipole on the gantry (AMF3), due to their long settling times. Rapid energy changes are, however, possible by making use of the beamline acceptance, provided that the impact of the altered energy spectra has a negligible effect on the beam characteristics at isocenter. Distortion in the energy spectra can, indeed, introduce modification in certain beam parameters, which would result in a lower quality of the treatment.

The beam properties for the energies used in clinical treatments are well characterized and undergo strict quality assurance tests.[28] Each beamline element is controlled using a lookup table of settings, so-called *tune*, calculated by interpolating each individual

element response for optimal beam transport to the treatment isocenter. Investigating the beam properties within the momentum acceptance requires overwriting these beamline *tunes*, such as to alter the beam energy spectra and beamline settings.

With reference to Figure 1, we will refer to E_m as the residual energy at the exit of the nozzle, derived from experimental range measurements and converted according to ICRU 49 energy range report and to E_s^D as the energy setpoint of the upstream degrader. Throughout the manuscript, the formalism is expanded to include reference to the specific energy band under consideration (*i*) and position within the acceptance (*j*), with *j* being equal to the number of steps within the acceptance band in steps of dp/p bounded by *low* (nominal energy – ½ dp/p) and *up* (nominal energy + ½ dp/p) at the boundaries of the acceptance.

Under these conditions, two options for energy modulation have been considered in this study:

- Upstream degradation: the entire beamline is tuned for the mean energy of the corresponding *i*th momentum acceptance band. The upstream degrader position is changed to modulate the beam energy within the band $E^D_{s,i,[low...up]}$.
- Local degradation: the beamline section up to the coupling point is tuned for the upper bound of the acceptance ($E^D_{s,i,up}$), whereas the gantry energy setpoint is equal to the mean energy of *i*th band ($E^D_{s,i,0}$). Since a local degrader is not available at the facility, beam energy has been degraded by manually inserting foils of variable thickness of polymethyl methacrylate (PMMA) at the coupling point.

For both scenarios, and unlike standard clinical operation, in our measurements, the momentum slits were kept open, maximizing the off-momentum particles transported through the beamline. Modulating the energy off, the mean value of each respective band results in changes in the beam radius of curvature at bending elements, so in the beam trajectory within the energy selection system. If not compensated for by a dipole retuning, such offset trajectory would be cause of significant transmission drop as a result of beam collisions with the momentum slits. By keeping the slits open, such losses are overcome at the price of broadening the energy spectrum of the beam.

For each degrader option, the following beam parameters have been investigated:

- Beam position and trajectory angle
- Distortions of the integral depth-dose profile and beam width

In addition, for the upstream degrader, a parameterization of the beam range and current within the acceptance band have been estimated. Finally, we also experimentally investigated the potential of in-acceptance-band energy modulation for an example clinical case. Those steps were not possible for the local degrader, which is not installed yet in our facility.

2.2 | Beam range parameterization within acceptance

Even though the mean beam energy is kept within acceptance, particles with extreme energies at the boundaries of the momentum band are lost due to collisions in the selection system and bending elements, modifying the energy spectra at the nozzle exit and consequently the range at isocenter. In order to model such a behavior, reference data have been taken for a set of 19 energy bands (*i*) between 150 and 228 MeV while setting up the beamline at the mean energy of each *i*th band and the upstream energy degrader in sequence at the lower bound (dp/p = –0.6%) of acceptance, mean acceptance band energy (dp/p = 0.0%), and upper bound (dp/p = +0.6%). Bands have been selected to be nominally consecutive, therefore, imposing that $E^D_{s,i,up} = E^D_{s,i+1,low}$. Beam ranges measured at isocenter with a multilayer ionization chamber (Giraffe MLIC, IBA Dosimetry, Schwarzenbruck, D) have been converted to corresponding energies via ICRU 49 energy-range tables. For setpoints other than the mean band energy, a mismatch can be observed between the energy requested from the machine ($E^D_{s,i,j}$) and actual measurements ($E_{m,i,j}$). Note, however, that despite ensuring energy continuity at the boundaries, the gaps between the measured energies of consecutive bands prevent continuous control of beam range at isocenter (Figure 2a).

Based on this set of experimental measurements, the beamline response has been modeled with the aim of defining a new set of bands allowing for theoretically seamless range control and the energy degrader correction offset required to implement energy regulation within the acceptance of our Gantry 2 treatment unit has been parameterized.

Our approach is based on the analysis of the delta between the energy measured at lower ($\Delta E_{m,i,low}$) and upper bounds ($\Delta E_{m,i,up}$) of each band with respect to the mean band energy ($E_{m,i,0}$) and calculation of the gradient of the line fitting these three points (*m-coefficient)*, approximating the beamline response within acceptance. A schematic interpretation of these three key parameters is given in Figure 2b.

2.2.1 | Finding a new set of bands

The generation of a new set of *tunes* for continuous range regulation requires the identification of a list of

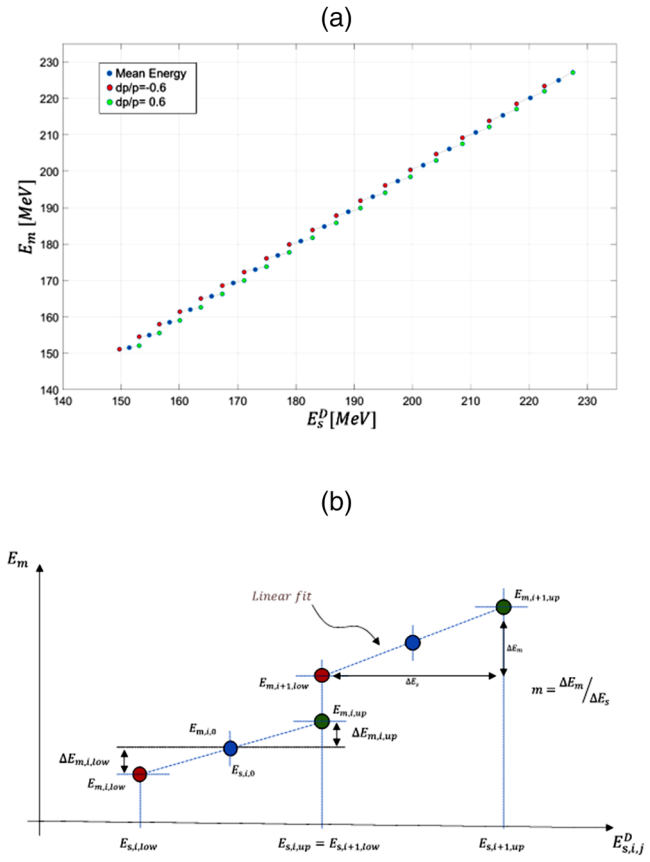

FIGURE 2 Panel (a), energy (E_m) corresponding to the measured range at isocenter as a function of the upstream energy degrader setpoint E_s^D for consecutive acceptance bands 1.2% dp/p wide from 150 to 228 MeV. Panel (b), schematic representation of key quantities used for beam range error modeling and compensation. The energy bands have been modeled to be linear: the blue markers represent the mean energy of the band, while the red and green ones represent, respectively, the lower and upper limits

mean energies whose band boundaries are contiguous. This is achieved by imposing the continuity of the energies measured at the edges of the bands, making the upper limit of each to coincide with the lower limit of the next, thus formally:

$$E_{m,i,up} = E_{m,i+1,low}$$

Starting from an arbitrary upper bound energy value ($E_{m,i,up}$) and assuming the low bound energy delta with respect to the mean energy of current band to be a good approximation for band that follows ($\Delta E_{m,i,low} \approx \Delta E_{m,i+1,low}$), the next band mean energy and upper bound can be calculated as follows:

$$E_{m,i+1,0} = E_{m,i,up} + \Delta E_{m,i,low}$$

$$E_{m,i+1,up} = E_{m,i+1,0} + \Delta E_{m,i+1,up}$$

Considering that at band mean the degrader setpoint coincides with the actual energy measurement, the calculated $E_{m,i,0}$ are the centers of a new band set allowing for seamless energy coverage with contiguous boundaries.

2.2.2 | Definition of degrader settings

Even though the potential for energy modulation within the acceptance drops progressively as the energy decreases, the effect is in a first approximation linear within each band (Figure 2). Such an effect has been parameterized by calculating the gradient coefficient (*m-coefficient*) of each band, modeling the beamline response as a function of the degrader setpoint $m(E^D_{s,i,0})$. Therefore, the *m*-parameterization links the setpoint energy requested from the machine ($E^D_{s,i,j}$) and the one actually measured at isocenter ($E_{m,i,j}$) within each band, and allows to compute the correct degrader setpoint for any arbitrarily chosen energy and vice versa, to estimate the expected energy at isocenter for a given degrader setpoint (*j*) within any band (*i*) whose mean energy is known.

For validation purposes, a refined list of contiguous bands defined as described in Section 2.2.1 has been verified at the boundaries and in steps of 0.2% dp/p around the mean energy. Estimated energies have been compared with actual range measurements taken at our institute using the setup introduced before, with the IBA Giraffe MLIC detector aligned at isocenter.

2.3 | Beam current parameterization within acceptance

Proton collisions in the beamline when varying the beam energy toward the edge of the momentum bands reduce beam transmission. Such current losses have been investigated by analyzing the delivery logfiles and comparing beam monitor readings at the exit of the cyclotron to those in the nozzle. The ratio of the two monitors as a function the mean band energy ($E^D_{s,i,0}$) has been parameterized within the 19 bands already considered for the beam range analysis (Section 2.2.1) between 228 and 150 MeV. The beam current has been sampled in steps of dp/p = 0.15% to fit a continuous correction function for the beam current in the considered energy range.

2.4 | Beam position and trajectory angle

The beam position at treatment isocenter is primarily determined by the sweeper magnets, which are tuned as a function of the beam energy. Therefore, variations in the energy spectra may introduce beam position errors, unless compensated for otherwise. We have verified the

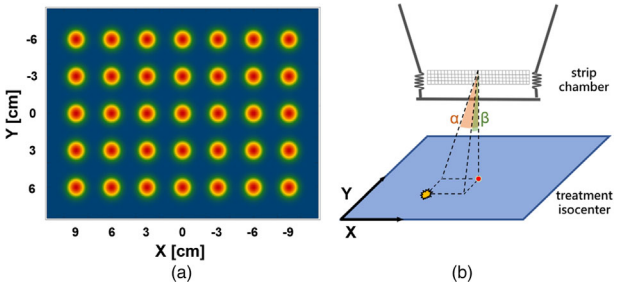

FIGURE 3 In panel (a), planned spot grid considered to assess beam position errors consisting of 35 spots on a 18 × 12 cm regular grid, respectively, in the X and Y directions. Panel (b): beam trajectory angle for an off-momentum beam. α and β are, respectively, the angles between the spot position in the strip and at isocenter in X and Y directions

extent of this effect for symmetrical energy variations at the extreme of the acceptance (dp/p = ± 0.6%, j = [low, up]) for three energies used on the PSI Gantry, namely, 150, 200, and 228 MeV. For the latter, the explored range has been reduced to dp/p = ± 0.4% (j = [–0.4, 0.4]), such as not to exceed the 230 MeV upper bound allowed in clinical settings at the facility. The alternative option of using a local degrader at the coupling point has also been investigated for a beam at 200 MeV. For this latter measurement, a selection of PMMA foils manually inserted at coupling point has been used to replicate the changes in beam range verified with the upstream degrader.

In the nozzle, the transversal beam position is monitored and measured with a strip monitor, equipped with two orthogonal planes of 2 mm wide strips and fast readout electronics. Beam position is determined by calculating the center-of-gravity of the strip profiles.[31] Moreover, an exact replica of the nozzle strip chambers has been aligned at treatment isocenter, 71.15 cm from the nozzle detector. The position of 35 dose spots, 3 cm apart on a 18 × 12 cm grid covering the entire scan range of Gantry 2 (Figure 3), was obtained from the mean of the Gaussian fit of the strip profiles. Monitor data acquired at the isocenter were compared with the corresponding data acquired at the mean energy band to quantify the in-plane error, and combined with beam positions measured in the nozzle to compute the beam trajectory angle.

2.5 | Distortions of the integral depth-dose profile and beam width

The larger beam energy spectra resulting from opening the momentum slits influences the Bragg peak shape, affecting both the depth-dose profile and beam width. The effects on both profiles have been investigated with dedicated measurements. Depth-dose curves and beam width have been measured for the same set of energies and degrader settings used for the assessment of beam position errors in Section 2.4: 150, 200, and 228 MeV for the upstream degrader and 200 MeV for the local degrader. Integral depth-dose curves were acquired with a large parallel-plate ionization chamber of 80 mm diameter immersed in a water tank. A motorized stage moved the chamber along the beam axis to sample the Bragg peak curve while delivering continuous beam at isocenter.[32] The measured relative depth-dose profiles were normalized to the dose at plateau, chosen as the dose at 2 cm depth in water. Experimental data were used to evaluate changes in depth-dose profile with respect to reference clinical data using 1D gamma analysis at 1%, 1 mm.

To assess changes in the lateral beam width, first the 2D beam profiles were measured with a scintillating screen coupled with a CCD camera (Apogee Alta U6, Roseville, CA, USA)[33] to evaluate the in-plane spatial sigma σ_x and σ_y. For each considered energy, data have been repeatedly acquired setting up the scintillating foil at three different positions, 9.9 cm below, 13.2 cm above, and at isocenter, to fully characterize the angular spatial distribution of the beam in air. As suggested by Safai et al.,[34] we considered the average spatial spread $\sigma_s \sim= \sqrt{\sigma_x \sigma_y}$, the Gaussian angular spread σ_θ, and its covariance $\sigma_{s\theta}$. However, when traversing tissues in clinical treatments, the beam size increases due to proton multiple coulomb scattering. Following analytical considerations, therefore,[35] the beam broadening in water has been added in quadrature to the beam sigma in air to estimate the total beam width at the Bragg peak.

2.6 | Degrader latency

The time performance of the upstream degrader has been investigated by analyzing machine log files. For safety reasons, during delivery, any change in the beamline settings has to be followed by an acknowledge message, signaling to the therapy control system that the required setpoint has been reached. Such a check is performed by independent systems, namely, the beamline run permit system and patient safety system, acting as a safety supervisor. In characterizing the degrader performance, we have (1) generated a plan without dose spots but only energy changes and (2) extended the granularity of the control system log files to quantify the degrader latency directly from the control system. In doing so, no dose or beam current checks have been overridden or excluded. Repeated measurements were analyzed for the same set of 19 bands and 0.15% dp/p steps considered in the beam current analysis (Section 2.3) with energy changes in a ramp-down sequence, going from the highest to the lowest.

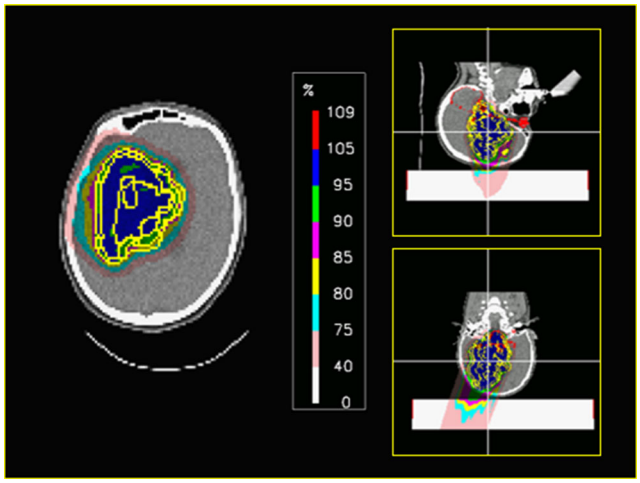

FIGURE 4 Head cancer patient treatment plan with a SFUD field and a cylindric range shifter (HU 3071) in the beam direction, above the patient head. Dose colorwash expressed as a percent of the prescription dose

2.7 | A clinical example

Finally, energy modulation within the momentum acceptance has been tested delivering a proton plan originally prepared for the treatment of a cranial glioma. The plan was optimized using the single-field uniform dose (SFUD) approach to deliver 1.8 Gy_{RBE} on a planning target volume (PTV) of 279.6 cm^3 in 48 energy layers from 122 to 103 MeV. Additional information regarding the plan and target geometry is given in Figure 4.

Plan characteristics:
Prescribed dose: 1.8 Gy**RBE**
CTV volume: 183.9 cm^3
PTV volume: 279.6 cm^3
Gantry angle (IEC): 90°
Patient support angle (IEC): 110°
Plan optimization: SFUD

Range shifter:
Thickness: 5.2 cm
Hounsfield Units: 3071

In order to make best use of the momentum acceptance, a simulated range shifter has been added next to the patient's head by editing the planning CT images. With 5.2 cm thickness and 3071 HU, such a structure increases the required energies for the plan by 92 MeV, using 214 MeV for the most distal layer. The plan has been delivered twice: (1) using the standard settings for clinical treatments and (2) making use of the beamline acceptance to reduce the number of full beamline tuning. For the latter case, each energy from the clinical plan has been assigned to a corresponding acceptance band, including range (Section 2.2.2) and beam transmission (Section 2.3) compensations, resulting in 19 out of the 48 original energy changes being implemented within acceptance and, therefore, not requiring changes of the beamline magnets.

Following our clinical protocol, a patient-specific calibration was performed. In an initial dummy run, both plans were delivered to a beam blocker and the recorded machine log files used to refine the sweeper magnets setting on a spot-by-spot basis in a process referred to as *teaching*.[23] Afterward, the plans have been verified using a cross-calibrated array of ionization chambers (PTW Octavius 1500XDR, Freiburg, D) aligned at isocenter. The measurement was performed at three depths located proximally, roughly in the middle and distally in the field. PMMA plates were piled on the dosimeter to measure transversal planes at 19.59, 23.74, and 28.19 cm water equivalent depths. Measured dose distributions have been compared to the standard plan (1) considered as reference, using the gamma 1%, 1 mm criteria for all points above 5% of the maximal dose of each plane.

3 | RESULTS

3.1 | Performance tests and clinical example for the upstream degrader

3.1.1 | Beam range parameterization within acceptance

The delta between the energy measured at lower ($\Delta E_{m,i,low}$) and upper bounds ($\Delta E_{m,i,up}$) of each band with respect to the mean band energy ($E_{m,i,0}$) was almost symmetrical up until the highest energies, with a difference between the two boundaries below 0.2 MeV. At higher energies, the symmetry was lost with a skew toward the upper bound, which measured about 30% more amplitude than the lower bound for the highest energy verified (225.1 MeV) (Figure 5a). For corresponding energies, the *m*-coefficient is a monotonically increasing function ranging from about 0.3 at lower bands where effective modulation is limited, up to 0.7 at higher energies (Figure 5b).

New beamline *tunes* including such a beam range compensation model have been verified using the upstream degrader available at the facility. Discrepancies between the setpoint energy and measured range at isocenter observed without compensation (Figure 2) were effectively compensated for, even though ensuring continuity in range required a higher number of bands and their overlaps. Continuous energy regulation from 150 to 229 MeV required the addition of 21 bands to the 19 considered previously. The range error distribution including the parameterized compensation is shown in Figure 6 at seven regular momentum steps within the energy acceptance. Residual errors quantified as the difference between estimated and measured beam range

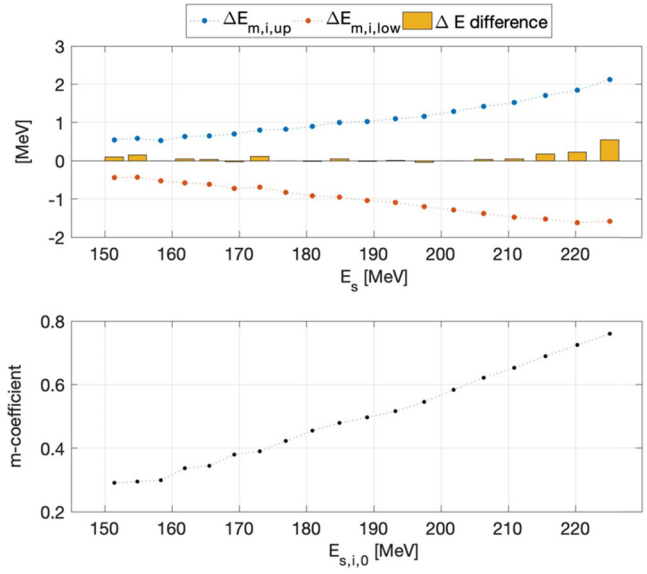

FIGURE 5 (a) Delta between measured energy at isocenter for the lower ($\Delta E_{m,i,low}$) and upper ($\Delta E_{m,i,up}$) bounds of the acceptance (±0.6% dp/p) with respect to the mean band energy from 150 to 228 MeV. (b) The corresponding gradient (m-coefficient) of the linear fit that relates the upstream degrader energy setpoint with the actual measured energy within each band

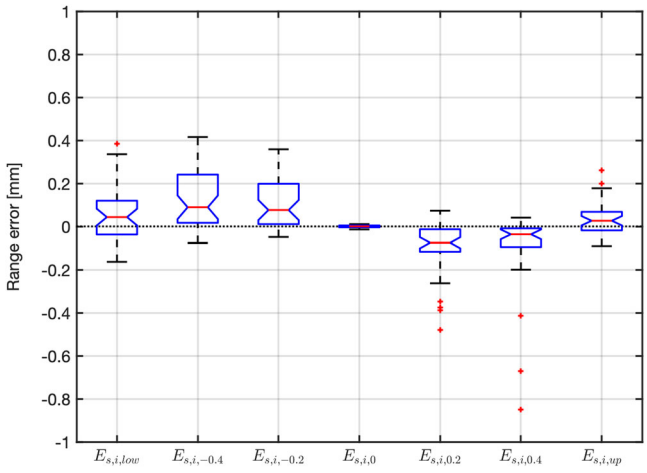

FIGURE 6 Distribution of range errors as difference between estimated and measured beam range at isocenter within acceptance, including a model for range compensation

at isocenter had a median of 0.05 mm (0.1 mm IQR) and were considered negligible for clinical applications.

3.1.2 | Beam current parameterization within acceptance

Following the model to compensate for the range gap existing within bands, the new beamline settings have been verified for transmission assessing the upstream/downstream beam current ratio. Seven measurements were taken sampling each momentum band at the same regular steps within the boundaries ($E_{s,i,low}$ and $E_{s,i,up}$) used for range analysis. Unlike range, however, the current loss was found to be nonlinear within the acceptance, dropping asymmetrically as the energy approaches the boundaries of the band. In Figure 7a, the current drop as a function of the momentum acceptance steps within all the energy bands is shown. The magnitude of beam loss, being a function of the band, thus of $E_{s,i,0}$, was larger at the lower energies but followed a similar trend in the whole considered range. B-spline interpolation has been used to fit beam losses of each band individually (Figure 7b) and extrapolate the current correction required to match the beam transmission of clinical operation. Overall, the root mean square error of the fit was 1.6% of the transmission ratio.

3.1.3 | Beam position and trajectory angle

The spot position errors for off-momentum particles are a function of the magnetic field set at the sweeper magnets, and for an upstream scanning system as the one considered in our study, the tuning of the last dipole magnet, which ultimately deflects the beam to the treatment isocenter. The interplay between these elements results in beam position errors, which vary across the scan range. Overall, errors increase toward the boundaries of the scan range for energies at the edge of the momentum acceptance and predominantly affect the dispersive beam direction (X coordinate). The measured spots' positions of the grid plan for energies at lower and upper edges of the acceptance are shown in Figure 8a for the 200 MeV band. Due to the complex combination of different factors to the final beam position, not least the tuning of the sweepers and design of the 90° bending magnet optic, the in-plane error does not have a minimum in the center of the field and increases moving toward the boundaries of the scan range (Figure 8—panel b). Even though beam position errors slightly above 1 mm with respect to the mean band energy were measured (Figure 8—panel b), those were found to be relatively symmetrical, with a difference within 0.25 mm between the two edges (Figure 8—panel c). Moreover, the beam angle was of larger magnitude in the dispersive direction (α) than in the transversal one (β), with measured maximal angular discrepancies, respectively, of 0.72 and 0.24 mrad with respect to beams at the mean band energy. Results for the 150 and 228 MeV bands follow a similar trend, data provided in the Appendix.

3.1.4 | Distortions of the integral depth-dose profile and beam width

The depth-dose curves for energies at the limit of the acceptance were only marginally distorted. Gamma

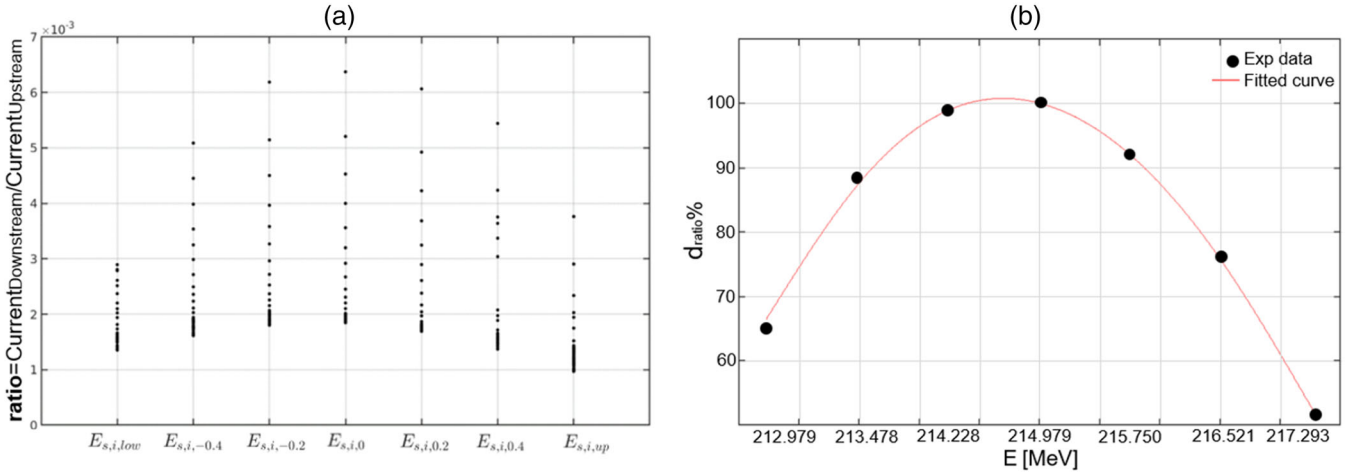

FIGURE 7 (a) Upstream/downstream beam current ratio measured within momentum bands, including range compensation (287 bands evaluated). (b) Exemplary transmission loss parameterization with smoothing spline functions from the dataset of mean energy of 214.979 MeV

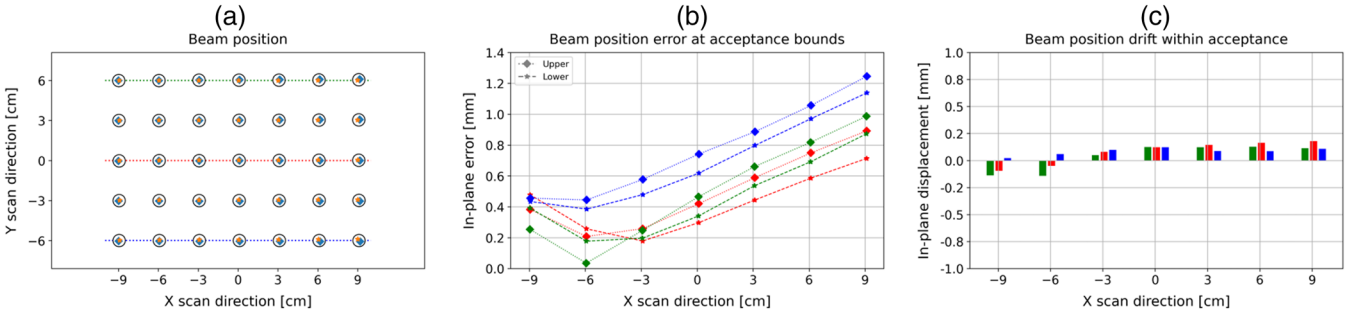

FIGURE 8 Analysis of beam position error within acceptance for an upstream degrader setup (200 MeV band, ±0.6% dp/p). Panel (a): absolute beam position across 18 × 12 cm scan range for mean energy (circle), lower (star), and upper (diamond) acceptance edges. Panel (b): 2D in-plane error at the acceptance edges with respect to mean band energy as a function of the spot position in the dispersive direction (X). Three transversal positions are shown at the boundaries (Y = –6, blue; 6 cm, green) and in the middle of the scan range (Y = 0 cm, red). Panel (c): difference of in-plane beam position errors measured at the edges of acceptance calculated as delta between the 2D error of beams at +0.6 and –0.6% dp/p

TABLE 2 Gamma pass rate (1%, 1 mm) with respect to mean band energy $E_{m,i,0}$ for beams at the limit of the acceptance (dp/p = ± 0.6%) for upstream ($E^{D}_{s,i,j}$) and local degrader ($E^{C}_{s,i,j}$) options

			Upstream degrader		Local degrader	
Mean band energy $E_{m,i,0}$ [MeV]	**$E^{D/C}_{s,i,j}$ [MeV]**	**dp/p**	**ΔR80 [mm]**	**Gamma (1%, 1 mm) pass rate**	**ΔR80 [mm]**	**Gamma (1%, 1 mm) pass rate**
228	229.648	+0.6%	+3.78	100%		
	226.356	–0.6%	–3.18	98.62%		
200	202.194	+0.6%	+2.51	91.82%	+2.44	97%
	197.815	–0.6%	–3.16	94%	–3.08	93.4%
150	151.680	+0.4%	+1.06	100%		
	148.328	–0.4%	–0.76	96%		

Note: Gamma evaluated after Bragg peak alignment by the ΔR80 shift. The dp/p has been reduced for the highest energy to ± 0.4% due to technical constraints.

pass rates have been calculated after Bragg peak alignment at 80% of the fall-off (ΔR80) of the non-nominal momentum beam under testing, that is, the measured energy corresponding to the degrader set-point $E^{D}_{s,i,j}$ and the profile of the mean band energy ($E_{m,i,0}$). Overall, as shown in Table 2, pass rates with a strict 1%, 1 mm criteria were all above 90%.

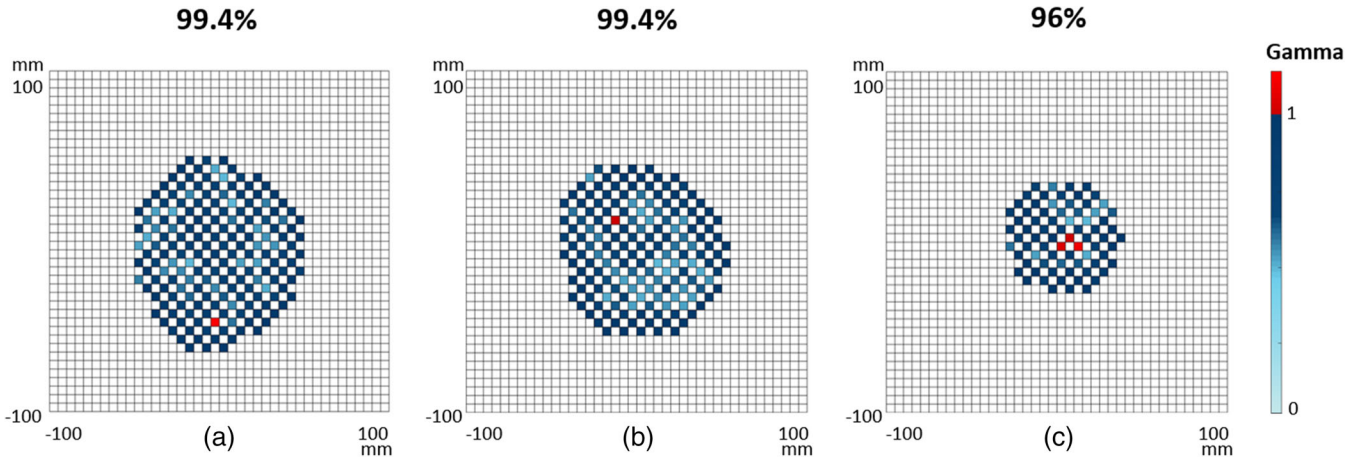

FIGURE 9 Gamma maps and pass rate at 1%, 1 mm for all chambers above 5% of the maximum dose of each measurement plane comparing the plan delivery with or without energy regulation within acceptance. Results given at three depths from a to c: proximal 19.59 cm, mid 23.74 cm, and distal 28.19 cm measurement planes

3.1.5 | Degrader latency

The latency of the upstream degrader has been assessed by analyzing 156 measurements in steps of dp/p = 0.15%, corresponding to shifts in water equivalent range from 2.4 to 0.7 mm in the considered energy range. The elapsed time between the request to change the degrader wedges' position and the execution notification sent by the system controller has been considered as a measure of latency. The median value, assessed in 10 repeated series of measurements, was determined to be 27.9 ms (IQR: 5.9 ms).

3.1.6 | A clinical example

Finally, based on ionization chamber array measurements for the applied clinical case, the worst results have been measured for the most distal plane, with a gamma pass rate of 96.0% at 1%, 1 mm (Figure 9, panel c), albeit still well within the clinical requirements. With our machine, the total delivery time was marginally shorter making use of acceptance for energy regulation (38.27 s) compared to the clinical settings (45.55 s), with a median energy change time, respectively, equal to 133.57 ms (IQR 27.79 ms) and 161.23 ms (IQR 35.04 ms) when considering all the energy layers, including those requiring full beamline tuning. Focusing instead on the 19 energy layers where the energy has been changed within the momentum acceptance, the median energy change time was, respectively, equal to 55.7 ms (11.4 ms) and 82.3 ms (14.2 ms), respectively, resulting in a reduction of 45.55% of the energy switching time. In Figure 10, the energy switching time for these selected layers is shown from two consecutive deliveries of the clinical example, confirming the reproducibility of the performance.

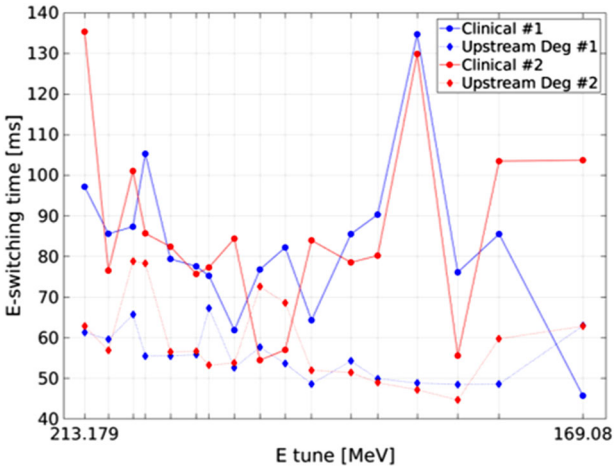

FIGURE 10 Energy switching time for a selection of energy layers using regulation within acceptance. The plan has been delivered twice using the clinical settings (Clinical #1 and Clinical #2) and twice making use of the momentum acceptance (Upstream Deg #1 and Upstream Deg #2)

3.2 | Preliminary comparison with a local degrader

3.2.1 | Beam position and trajectory angle

Spot positions measured around the 200 MeV band are shown in Figure 11a. Similarly to what observed for the upstream degrader setup, errors of larger magnitude were measured along the X scan direction and at the boundaries of the scan range. The different beamline setup, however, has implication on the error distribution across the field (Figure 11—panel b) with peak values marginally higher than the upstream degrader settings and to a larger extent on the error symmetry, or lack of thereof, with respect to the mean band

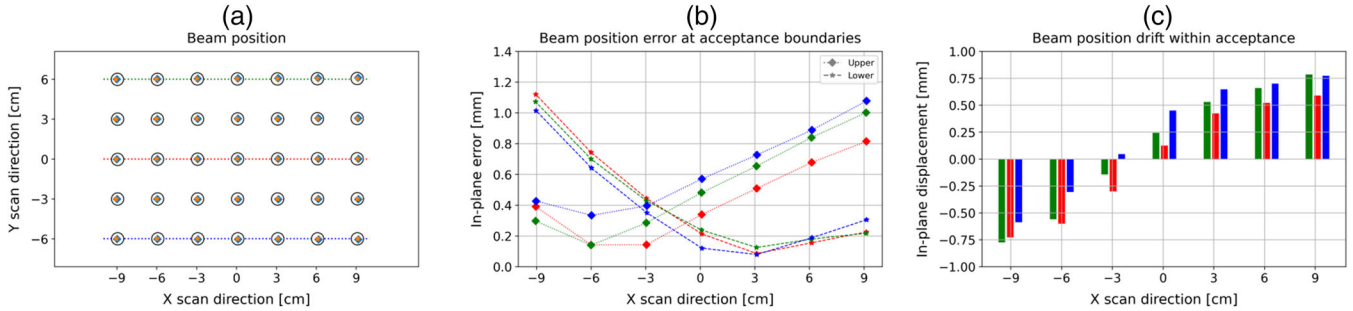

FIGURE 11 Analysis of beam position error within acceptance for the local degrader setup (200 MeV band, ±0.6% dp/p). Panel (a): absolute beam position across 18 × 12 cm scan range for mean energy (circle), lower (star), and upper (diamond) acceptance edges. Panel (b): 2D in-plane error at the acceptance edges with respect to mean band energy as a function of the spot position in the dispersive direction (X). Three transversal positions are shown at the boundaries (Y = –6, blue; 6 cm, green) and in the middle of the scan range (Y = 0 cm, red). Panel (c): difference of in-plane beam position errors measured at the edges of acceptance calculated as delta between the 2D error of beams at +0.6% and –0.6% dp/p

energy (Figure 11—panel c). Angular discrepancy with respect to beams at the mean band energy was of larger magnitude in the dispersive (α) than transversal (β) direction, with, respectively, up to 0.95 and 0.31 mrad α and β angles.

3.2.2 | Distortions of the integral depth-dose profile and beam width

As already observed for the upstream degrader, depth-dose curves for energies at the limit of the acceptance were also only marginally distorted using regulation at the coupling point. Absolute ranges in water for the local degrader were slightly different from those taken using the standard upstream system, as it was not possible to replicate exactly the amount of degrading material with PMMA foils. The difference was, however, of the same order as the measurement error expected in our experimental setup (0.1 mm). Nevertheless, this has been compensated for by calculating gamma pass rates after Bragg peak alignment at 80% of the fall-off (ΔR80) of the investigated non-nominal energies with $j \neq 0$ and the profile of the mean band energy ($E_{m,i,0}$). Overall, pass rates at strict 1%, 1 mm criteria were all above 90%, with no significant differences between the two degrader options (Table 2).

Finally, beam width has been measured in both the in-plane directions (X and Y in Figure 2), to calculate the angular spatial distribution at isocenter (Table 3). Both the angular $\Delta\sigma_\theta$ and the spatial $\Delta\sigma_s$ differences with respect to clinical references at corresponding energies were larger in absolute value for the local degrader with respect to the upstream one, as multiple Coulomb scattering in the local degrader material and after collimation produced larger beam sizes, beam divergence, and covariance. Indeed, beam size σ_s for the local degrader increased as a function of the amount of PMMA at the coupling point, whereas the upstream degrader σ_s had less variance and was closer to the clinical reference.

Overall, measured spatial beam broadening in air of non-nominal momentum beams was submillimetric for both degrader options. The ratio between the beam sigma when performing energy regulation within acceptance and the clinical beam settings was equal to 0.5%, 3%, and 4%, respectively, for the upper bound of the band, mean band energy of 200 MeV, and the lower bound, respectively.

4 | DISCUSSION

Proton beam properties have been characterized to investigate the clinical feasibility of fast energy modulation within the momentum acceptance of a medical beamline. In particular, we have focused on: beam shape and position, energy switching time and parameterization of range, and beam current corrections. Although the Gantry 2 beamline momentum acceptance is limited (dp/p = 1.2%), this is representative of current state-of-the-art proton therapy facilities.

As a general rule, beam position errors larger than 1–2 mm are clinically not acceptable.[36] For both upstream and local degrader settings, the errors increase approaching the edge of the acceptance and the boundaries of the scan range (Figures 8 and 11); and remain acceptable in the central part of the scanning area. Even though the scan range at PSI Gantry 2 is 20 × 12 cm, in this work, we have commissioned a smaller region of 18 × 12 cm to ensure accurate measurements, even in the presence of potentially large beam position errors. While modulating the energy within the acceptance, the sweeper magnets are calibrated for the mean band energy and, therefore, suboptimal precision in beam deflection has to be expected. This combines with the off-tuning of the 90° bending magnet, which

TABLE 3 Spatial spread ($\Delta\sigma_s$), angular spread ($\Delta\sigma_\theta$), and covariance ($\Delta\sigma_{s\theta}$) differences with respect to clinical reference at corresponding energy

	E [MeV]	$\Delta\sigma_s$ [mm]	$\Delta\sigma_\theta$ [mrad]	$\Delta\sigma_{s\theta}$ [mm * mrad]
Upstream Degrader	229.648	0.02 (0.7%)	0.003 (0.07%)	0.44 (11%)
	226.356	0.003 (0.1%)	0.1 (2.8%)	–0.66 (–16.3%)
	202.194	0.04 (1.4%)	0.2 (4.9%)	0.47 (9.9%)
	197.815	0.02 (0.7%)	0.16 (4%)	–0.57 (–11.3%)
	151.680	0.03 (0.8%)	0.03 (0.6%)	0.12 (1.4%)
	148.328	0.03 (0.8%)	0.07 (1.5%)	–0.15 (–1.7%)
Local Degrader	202.194	0.08 (2.9%)	0.05 (1.4%)	0.42 (8.9%)
	200	0.49 (18.8%)	0.8 (21.2%)	2.99 (62.9%)
	197.815	0.59 (22.8%)	1.16 (28.6%)	4.4 (87.2%)

Note: Values in brackets represent the percentage difference with respect to such reference values.

amplifies the magnitude of the error for an upstream scanning facility. This effect is visible in Figure 8a, where beams at lower energy drift inward in the isocenter plane. The complex contribution of various beamline elements to the position error hampers its modeling with a parameterization of general validity or extrapolation of results for larger scan ranges. Based on our data, however, a local degrader, introducing asymmetries in the beam position error within the acceptance (Figure 11—panel c), may require more sophisticated correction models than a setup making use of upstream energy degradation. However, and as shown in the clinical example, the refinement of the sweeper map calibration is possible and does not add dead time on the system latency. This procedure is in fact an integral part of the clinical workflow at our Gantry 2 facility.[23]

For the highest energy bands considered in this work (mean energy $E_{s,i,0} = 228$ MeV), range corrections of up to 7 mm could be achieved without changing the beamline magnet settings. As shown in Figure 2, however, within acceptance, the range changes are not directly proportional to the degrader settings, but instead require further modeling of machine performance when transporting off-momentum beams. Despite that changing energy without re-setting the beamline magnets can cause a misalignment of the proton beam, which, in turn, may result in asymmetric cuts of the spectra due to collisions, we have observed almost symmetric range variations for positive and negative momentum changes. This predictable response has facilitated the beamline modeling with a linear m-parameterization as a function of the transported beam energy, thus improving the control of range.

Unlike beam range, distortions in depth-dose profiles did not show an energy dependency in our experiments. Even for a strict gamma evaluation criterion at 1%, 1 mm, no significant differences have been observed between the two degrading options and the clinical references. Lateral beam width instead was larger using the local degrader and as a function of the degrading material thickness, with errors about one order of magnitude higher than upstream regulation. For the upstream degrader, even in the absence of dedicated collimation elements, the beam broadening does not contribute substantially to the beam size at target depth, while for the local degrader, the need for a dedicated strategy cannot be excluded.

Being a function of the beamline acceptance, the effectiveness of energy modulation naturally scales with energy, such that at the lower-end of the clinical ranges (70 MeV), it becomes so small as to be meaningless. For this reason, energies lower than 150 MeV have not been considered in this study. Instead, we have investigated the use of compensating material close to the patient in order to be able to exploit higher energies through the gantry and the larger range variation that can be achieved when modulating within the acceptance window.[37] In the clinical example, a dense material was used to offset the plan's energies, whose properties and contribution to beam broadening would require further investigation before its clinical implementation. Nevertheless, the dose distribution measured when varying beam energy within beamline acceptance had only negligible distortions compared to the clinical plan.

Although here we have explored the potential of a limited momentum acceptance, upstream energy modulation is, however, an interesting option. New medical beamline designs, featuring superconductive magnets, are under investigation, obviating the need for regulating dipole settings, while, nevertheless, allowing for energy regulation within large acceptances.[4] Recent studies on superconductivity have, indeed, opened up to the possibility of 15% or more[38] momentum acceptance in the future.[39] With large acceptance, almost no magnetic field changes would be required on dipoles to transport particles of different energy through the beamline,[38] substantially cutting down the time required for beam

energy modulation. In such a case indeed, not only energy could be continuously regulated without the need of downstream devices, but meaningful range corrections would be possible also at lower energies. Nevertheless, despite being limited at 1.2% dp/p, this momentum acceptance already gave us the possibility to reduce the number of magnet tune changes to 29 with respect to the 48 required by the current clinical operations. Considering a single momentum band around 225 MeV, up to three changes of beamline settings could be skipped by regulating the energy within the acceptance band covering 227.5–222.65 MeV range.

Fast energy modulation is of great interest across the particle therapy community, especially in the context of improving treatment efficiency. As reported in Table 1, there is a large variability in the performance of running facilities, ranging from hundreds of milliseconds to seconds for a change in beam energy. The fastest, nongantry solution is installed at the fixed beamline for carbon ion therapy at GSI, allowing for 5 mm beam range variation in 16 ms under experimental settings.[40] The use of a downstream, wedge-based beam degrader, however, is suboptimal for a proton clinical facility due to the substantially increased scattering of protons. Moreover, its integration into treatment rooms equipped with a rotating gantry is particularly difficult, making a retrofit on operational facilities impractical. On the other hand, the upstream regulation methods studied in this work do not require substantial modifications of the beamline and are, therefore, theoretically applicable in most running centers, not only in the cyclotron-based ones but also in treatment centers using synchrotrons: this is of particular interest because of the typically longer times required to modulate the beam energy.

The PSI Gantry 2 facility is one of the fastest machines in operation as regards energy changes, with a dead time in the order of hundreds of milliseconds. In this work, this could be reduced even further, down to 27 ms on average for small regulations within the momentum acceptance, while preserving clinical-level beam quality. This performance, however, does not find a full confirmation in the delivery of a clinical plan with only 6 s reduction of delivery time. Replicating the high performance achieved under experimental settings in the clinic, indeed, requires further development in the control system and communication with the beamline elements such as to guarantee treatment safety. In particular, direct control of the degrader by the therapy control system could be necessary to translate our experimental results to clinical applications. The gain, however, might be immediately relevant in facilities with slower energy layer switching times, in which case skipping energy changes may substantially reduce delivery times. Indeed, comparing only those energy layers where the momentum acceptance was exploited, energy switching time has been decreased by exploiting the momentum acceptance by 45% with respect to standard clinical settings.

Finally, the possibility to achieve fast energy modulation using the beamline momentum acceptance has a yet unexplored potential in the treatment of moving targets. Motion mitigation techniques like gating or rescanning increase substantially the delivery time and would benefit from a reduction in the energy switching time. Moreover, fast and continuous energy changes find a natural application in tumor tracking, where rapid changes in depth are fundamental to implement beam offset such as to follow the tumor motion.[3]

5 | CONCLUSIONS

The potential of energy regulation within momentum acceptance has been investigated on a gantry-based medical beamline. Provided that range and transmission losses introduced by the distortion of the beam spectra are compensated for, fast energy changes could be achieved under experimental settings while preserving clinical beam quality. While the use of local energy degradation poses further questions regarding beamline optimization, the more conventional upstream energy degradation already allows for fast energy changes in clinical treatments, with negligible distortions in the delivered dose distribution. Centers with slow energy switching time can particularly profit from such a technique for reducing dead time during treatment delivery.

CONFLICT OF INTEREST

The authors declare that there is no conflict of interest that could be perceived as prejudicing the impartiality of the research reported.

DATA AVAILABILITY STATEMENT

The data will be available to interested researches upon request and under a confidentiality agreement, as they contain sensitive information about a PSI product.

This study was supported by the Swiss National Science Foundation with the grant 185082 New concept for adaptive real time tumor tracking.

REFERENCES

1. Pedroni E, Bacher R, Blattmann H, et al. The 200-Mev proton therapy project at the Paul Scherrer Institute: conceptual design and practical realization. *Med Phys*. 1995;22(1):37-53. https://doi.org/10.1118/1.597522.
2. Haberer T, Becher W, Schardt D, Kraft G. Magnetic scanning system for heavy ion therapy. *Nucl Instruments Methods Phys Res A*. 1993;330(1-2):296-305.
3. Fattori G, Zhang Y, Meer D, Weber DC, Lomax AJ, Safai S. The potential of Gantry beamline large momentum acceptance for real time tumour tracking in pencil beam scanning proton therapy. *Sci Rep*. 2020;10(1):15325. https://doi.org/10.1038/s41598-020-71821-1.

4. Gerbershagen A, Meer D, Schippers JM, Seidel M. A novel beam optics concept in a particle therapy gantry utilizing the advantages of superconducting magnets. *Z Med Phys*. 2016;26(3):224-237. https://doi.org/10.1016/j.zemedi.2016.03.006.
5. Van De Water S, Kooy HM, Heijmen BJM, Hoogeman MS. Shortening delivery times of intensity modulated proton therapy by reducing proton energy layers during treatment plan optimization. *Int J Radiat Oncol Biol Phys*. 2015;92(2):460-468. https://doi.org/10.1016/j.ijrobp.2015.01.031.
6. Ohara K, Okumura T, Akisada M, et al. Irradiation synchronized with respiration gate. *Int J Radiat Oncol Biol Phys*. 1989;17(4):853-857. https://doi.org/10.1016/0360-3016(89)90078-3.
7. Hanley J, Debois MM, Mah D, et al. Deep inspiration breath-hold technique for lung tumors: the potential value of target immobilization and reduced lung density in dose escalation. *Int J Radiat Oncol Biol Phys*. 1999;45(3):603-611. https://doi.org/10.1016/S0360-3016(99)00154-6.
8. Zenklusen SM, Pedroni E, Meer D. A study on repainting strategies for treating moderately moving targets with proton pencil beam scanning at the new Gantry 2 at PSI. *Phys Med Biol*. 2010;55(17):5103-5121. https://doi.org/10.1088/0031-9155/55/17/014.
9. Schätti A, Zakova M, Meer D, Lomax AJ. The effectiveness of combined gating and re-scanning for treating mobile targets with proton spot scanning. An experimental and simulation-based investigation. *Phys Med Biol*. 2014;59(14):3813-3828. https://doi.org/10.1088/0031-9155/59/14/3813.
10. Mori S, Inaniwa T, Furukawa T, Zenklusen S, Shirai T, Noda K. Effects of a difference in respiratory cycle between treatment planning and irradiation for phase-controlled rescanning and carbon pencil beam scanning. *Br J Radiol*. 2013;86(1028):20130163. https://doi.org/10.1259/bjr.20130163.
11. Mizushima K, Furukawa T, Iwata Y, et al. Performance of the HIMAC beam control system using multiple-energy synchrotron operation. *Nucl Instruments Methods Phys Res Sect B Beam Interact with Mater Atoms*. 2017;406:347-351. https://doi.org/10.1016/j.nimb.2017.03.051.
12. Saito N, Bert C, Chaudhri N, et al. Speed and accuracy of a beam tracking system for treatment of moving targets with scanned ion beams. *Phys Med Biol*. 2009;54(16):4849-4862. https://doi.org/10.1088/0031-9155/54/16/001.
13. Pedroni E, Bearpark R, Böhringer T, et al. The PSI Gantry 2: a second generation proton scanning gantry. *Z Med Phys*. 2004;14(1):25-34. https://doi.org/10.1078/0939-3889-00194.
14. Weber U, Becher W, Kraft G. Depth scanning for a conformal ion beam treatment of deep seated tumours. *Phys Med Biol*. 2000;45(12):3627-3641. https://doi.org/10.1088/0031-9155/45/12/309.
15. Bert C, Rietzel E. 4D treatment planning for scanned ion beams. *Radiat Oncol*. 2007;2:24. https://doi.org/10.1186/1748-717X-2-24.
16. Smith A, Gillin M, Bues M, et al. The M. D. Anderson proton therapy system. *Med Phys*. 2009;36(9):4068-4083. https://doi.org/10.1118/1.3187229.
17. Shen J, Tryggestad E, Younkin JE, et al. Technical Note: using experimentally determined proton spot scanning timing parameters to accurately model beam delivery time. *Med Phys*. 2017;44(10):5081-5088. https://doi.org/10.1002/mp.12504.
18. Younkin JE, Bues M, Sio TT, et al. Multiple energy extraction reduces beam delivery time for a synchrotron-based proton spot-scanning system. *Adv Radiat Oncol*. 2018;3(3):412-420. https://doi.org/10.1016/j.adro.2018.02.006.
19. Biscari C, Falbo L. Medical applications. In: *Proceedings of the CAS-CERN Accelerator School: Advanced Accelerator Physics*. 2013. https://doi.org/10.5170/CERN-2014-009.487
20. Pidikiti R, Patel BC, Maynard MR, et al. Commissioning of the world's first compact pencil-beam scanning proton therapy system. *J Appl Clin Med Phys*. 2018;19(1):94-105. https://doi.org/10.1002/acm2.12225.
21. Farr JB, Flanz JB, Gerbershagen A, Moyers MF. New horizons in particle therapy systems. *Med Phys*. 2018;45(11):e953-e958. https://doi.org/10.1002/mp.13193.
22. Koschik A, Bula C, Duppich J, et al. Gantry 3: further development of the PSI PROSCAN proton therapy facility. In: *6th International Particle Accelerator Conference, IPAC 2015*. 2015.
23. Safai S, Bula C, Meer D, Pedroni E. Improving the precision and performance of proton pencil beam scanning. *Transl Cancer Res*. 2012;1(3):196-206. https://doi.org/10.3978/j.issn.2218-676X.2012.10.08.
24. Bula C, Meer D, Pedroni E. A system for the delivery of proton therapy by pencil beam scanning of a predeterminable volume within a patient. 2013.
25. Pedroni E. System for the delivery of proton therapy. 2009.
26. Klein HU, Baumgarten C, Geisler A, et al. New superconducting cyclotron driven scanning proton therapy systems. *Nucl Instruments Methods Phys Res Sect B Beam Interact with Mater Atoms*. 2005. 241(1-4):721-726. https://doi.org/10.1016/j.nimb.2005.07.123.
27. Bula C, Belosi MF, Eichin M, Hrbacek J, Meer D. Dynamic beam current control for improved dose accuracy in PBS proton therapy. *Phys Med Biol*. 2019;64(17):175003. https://doi.org/10.1088/1361-6560/ab3317.
28. Pedroni E, Meer D, Bula C, Safai S, Zenklusen S. Pencil beam characteristics of the next-generation proton scanning gantry of PSI: design issues and initial commissioning results. *Eur Phys J Plus*. 2011;126:66. https://doi.org/10.1140/epjp/i2011-11066-0.
29. Ma C-MC. *Proton and carbon ion therapy*. 2012. https://doi.org/10.1201/b13070
30. Maradia V, Meer D, Weber DC, Lomax AJ, Schippers JM, Psoroulas S. A new emittance selection system to maximize beam transmission for low-energy beams in cyclotron-based proton therapy facilities with gantry. *Med Phys*. 2021;48(12):7613-7622. https://doi.org/10.1002/mp.15278.
31. Actis O, Meer D, König S. Precise on-line position measurement for particle therapy. *J Instrument*. 2014;9(12). https://doi.org/10.1088/1748-0221/9/12/C12037.
32. Psoroulas S, Meer D, Oponowicz E, Owen H. Mean excitation energy determination for Monte Carlo simulations of boron carbide as degrader material for proton therapy. *Phys Med*. 2020;80:111-118. https://doi.org/10.1016/j.ejmp.2020.09.017.
33. Boon SN, van Luijk P, Böhringer T, et al. Performance of a fluorescent screen and CCD camera as a two-dimensional dosimetry system for dynamic treatment techniques. *Med Phys*. 2000;27(10):2198-2208. https://doi.org/10.1118/1.1289372.
34. Safai S, Bortfeld T, Engelsman M. Comparison between the lateral penumbra of a collimated double-scattered beam and uncollimated scanning beam in proton radiotherapy. *Phys Med Biol*. 2008;53(6):1729-1750. https://doi.org/10.1088/0031-9155/53/6/016.
35. Pedroni E, Scheib S, Böhringer T, et al. Experimental characterization and physical modelling of the dose distribution of scanned proton pencil beams. *Phys Med Biol*. 2005;50(3):541-561. https://doi.org/10.1088/0031-9155/50/3/011.
36. Psoroulas S, Bula C, Actis O, Weber DC, Meer D. A predictive algorithm for spot position corrections after fast energy switching in proton pencil beam scanning. *Med Phys*. 2018;45(11):4806-4815. https://doi.org/10.1002/mp.13217.
37. Titt U, Mirkovic D, Sawakuchi GO, et al. Adjustment of the lateral and longitudinal size of scanned proton beam spots using a pre-absorber to optimize penumbrae and delivery efficiency. *Phys*

Med Biol. 2010;55(23):7097-7106. https://doi.org/10.1088/0031-9155/55/23/S10.
38. Nesteruk KP, Calzolaio C, Meer D, Rizzoglio V, Seidel M, Schippers JM. Large energy acceptance gantry for proton therapy utilizing superconducting technology. *Phys Med Biol*. 2019;64(17):175007. https://doi.org/10.1088/1361-6560/ab2f5f.
39. Brouwer L, Huggins A, Wan W. An achromatic gantry for proton therapy with fixed-field superconducting magnets. *Int J Mod Phys A*. 2019;34(36):1942023.
40. Bert C, Gemmel A, Saito N, et al. Dosimetric precision of an ion beam tracking system. *Radiat Oncol*. 2010;5:61. https://doi.org/10.1186/1748-717X-5-61.

SUPPORTING INFORMATION

Additional supporting information may be found in the online version of the article at the publisher's website.

How to cite this article: Giovannelli AC, Maradia V, Meer D, et al. Beam properties within the momentum acceptance of a clinical gantry beamline for proton therapy. *Med Phys*. 2022;49:1417–1431. https://doi.org/10.1002/mp.15449